PAPER

The structural, electronic and catalytic properties of Au$_n$ ($n = 1$–4) nanoclusters on monolayer MoS$_2$

Hui Zhang,[a] Jia Zhu, [ID] *[a] Hongge Zhang,[a] Jinyan Zhang,[a] Yongfan Zhang[bc] and Zhang-Hui Lu [ID] *[a]

The structural stability, electronic and catalytic properties of Au$_n$ ($n = 1$–4) nanoclusters supported on monolayer MoS$_2$ have been investigated based on first principle DFT calculation with van der Waals (vdW) corrections. Our results show that all Au$_n$ ($n = 1$–4) nanoclusters prefer to bind vertically on the top S sites of the monolayer MoS$_2$. And the relative stability of Au$_n$ ($n = 1$–4) clusters in gas phase is not preserved after landing on monolayer MoS$_2$. By including van der Waals (vdW) corrections with different approaches, we found that the van der Waals correction increased the adsorption energies for all supported Au$_n$ ($n = 1$–4) clusters with the order of E_{ads}(PBE-D2) > E_{ads}(PBE-D3) > E_{ads}(optB86b-vdW) > E_{ads}(PBE). And the van der Waals effects can also change the order of stability and the energy differences of various deposition configurations. In addition, the binding of O$_2$ is also modeled, showing significantly enhanced adsorption properties and catalytic activation toward O$_2$ adsorption, especially for that on supported Au$_1$ and Au$_3$ clusters with magnetic properties, with respect to that on supported Au$_2$ and Au$_4$ clusters with nonmagnetic properties. The current study provides further insight into the adsorption and catalytic properties of small gold clusters supported on monolayer MoS$_2$, which play a crucial role in the activation of O$_2$.

1 Introduction

Supported gold nanoclusters have attracted considerable interest due to their unexpected catalytic properties in contrast with the inactivity of larger-sized particles or bulk gold.[1,2] In the past few years, they have been widely applied in heterogeneous catalysis field to catalyze many reactions, such as low temperature CO oxidation,[3–5] water-gas shift (WGS) reaction[6,7] and the oxidation of alkenes.[8] It is revealed that the chemical properties and catalytic activity of supported gold nanoclusters are dramatically depended by the size and shape of gold nanoclusters,[9–12] the structural fluxionality,[13–15] and the forms of the supported materials.[10,16–18] Recent experimental and theoretical works have focused on the effects of support materials on modifying/activating Au clusters by comparing various substrates including MgO,[18] TiO$_2$,[19] SiO$_2$,[20] CeO$_2$,[21] and Fe$_2$O$_3$.[22] In particular, it is demonstrated that the different charged gold cluster is one of the origins for the high catalytic activity of supported gold nanoclusters. Well characterized examples are those of negative charged gold nanoclusters forming when gold clusters deposited on TiO$_2$, defect MgO and CeO$_2$, result in

activation of O$_2$ molecules for further catalytic reaction or dissociation.[18,20,21] On the other hand, after adsorption on Fe$_2$O$_3$ and SiO$_2$ surface the gold nanoclusters become positive charged, which promote adsorption of other reactants, such as CO and hydrocarbons.[20,22,23] It is indicated that the catalytic activity of gold clusters are strongly influenced by the types of support materials. Therefore, the choice of suitable support is crucial for a rational design of chemical properties and activities of supported gold clusters.

In the past few years, a continuously increasing interest have been devoted to two-dimensional nanomaterials, such as graphene, silicene, hexagonal boron nitride (h-BN), TiO$_2$ nanosheet, serving as excellent candidates of the support of metal nanoparticles for enhancing adsorption performances and catalytic properties of metal catalysts, because of their extraordinary physical, chemical and optical properties.[24–31] For example, graphene has been shown to be an excellent substrate material for dispersion of the transition metal (TM) nanoparticles, due to its large surface areas, outstanding electronic and thermal conductivity, as well as the high mechanical strength and low production cost.[32,33] Theoretically calculation showed that supported gold clusters on h-BN surface can considerably enhance their adsorption and catalytic activity of adsorbed O$_2$ molecule.[28] On the other hand, the great advance in two-dimensional-based nanomaterials research has encouraged scientists to explore other two-dimension-based materials. Among them, one emerging class of transition metal

[a]*College of Chemistry and Chemical Engineering, Jiangxi Normal University, Nanchang, Jiangxi 330022, China. E-mail: jia_zhu@jxnu.edu.cn; luzh@jxnu.edu.cn*

[b]*Department of Chemistry, Fuzhou University, Fuzhou, Fujian, 350108, China*

[c]*State Key Laboratory of Photocatalysis on Energy and Environment, Fuzhou, Fujian, 350002, China*

dichalcogenides (TMDs), monolayer molybdenum disulfide (MoS_2) has been a recent hot topic. Indeed, monolayer MoS_2 is a semiconductor with a direct band gap of 1.9 eV,[34] which are associated with large surface areas and abundant active sites.[35,36] The experimental results from Xia *et al.* suggested that Au nanorods deposited on MoS_2 nanosheets activates the electrocatalytic activity for hydrogen evolution reaction (HER).[37] However, very little attention has been paid to theoretical investigation concerning the role of the MoS_2 support on the chemical and catalytic properties of gold nanoparticles. The structural, electronic properties, and catalytic activation of supported gold clusters on monolayer MoS_2 are also not obtained, which is very essential for investigating the cluster-support interaction effects, interface structure, as well as the charge transfer between supported gold cluster and substrate. In addition, van der Waals (vdW) forces are ubiquitous in the binding of atoms and molecules. In the past few years accurately accounting for van der Waals (vdW) forces and understanding the role they play in extended systems have become a thriving topic of research, which play a crucial role in improvement of theoretical description for those systems.[34,38,39]

In this work, by performing first principles DFT, we investigate the structures and electronic properties of Au_n ($n = 1–4$) clusters supported on monolayer MoS_2 including the van der Waals (vdW) forces correction. Furthermore, to further understand the modification/activation of gold nanoclusters on monolayer MoS_2, the adsorption behaviors of O_2 on Au_n ($n = 1–4$)/MoS_2 are also determined. The paper is organized as follows. We first study the gas-phase Au_n ($n = 1–4$) clusters. Then, we investigate the structures and electronic properties of Au_n ($n = 1–4$) clusters supported on monolayer MoS_2 with DFT results. Furthermore, the effects of the van der Waals corrections using several vdW inclusive DFT schemes (PBE-D2, PBE-D3 and optB86b-vdW) are discussed. Finally, we discussed the adsorption and activation behaviors of O_2 molecule on Au_n ($n = 1–4$)/MoS_2 systems, which can help for further insight into adsorption and catalysis properties of small gold clusters supported on monolayer MoS_2.

2 Computational details

Spin-polarized density functional theory (DFT) calculations were performed using the Vienna Ab initio Simulation Package (VASP)[40–42] and the projected augmented wave (PAW) methods.[43,44] The generalized gradient approximation of Perdew, Burke and Ernzerhof (PBE) functional[45] was employed to treat the exchange-correlation energy of interaction electrons. The kinetic energy cutoff for the plane-wave expansion was set to 400 eV. A ($3 \times 3 \times 1$) Monkhorst–Pack (MP) mesh was used for the *k*-point sampling of the Brillouin zone. To calculate the projected density of states (PDOS), the set of *k*-points was adjusted to ($5 \times 5 \times 1$). The lattice parameter of monolayer MoS_2 was optimized to be 3.18 Å, which is in good agreement with the experimental (3.20 Å [46]) and theoretical values (3.18 Å,[47,48] 3.19 Å,[49] 3.20 Å [50]). To accommodate various sizes of the gold clusters, a (5×5) supercell consisting of 75 atoms (50 S atoms and 25 Mo atoms) was introduced. The supercell size of the monolayer MoS_2 has been tested and the (5×5) supercell is

large enough to obtain the properties focused on the present work. During the geometry optimization all the atoms in the monolayer MoS_2 were relaxed in all directions.

For Au_1 and Au_2 clusters, we started by placing the Au_1 and Au_2 clusters on different sites of monolayer MoS_2 as different adsorption models. Then these initial geometries were optimized using above settings. Since the ground states of Au_3 and Au_4 clusters in gas phase are V-shaped[51] and rhombic[52] structures, respectively. We first place these two clusters on the monolayer MoS_2 as initial structures. The deposition of Au_3 and Au_4 clusters on the monolayer MoS_2 are more complicated with many possible arrangements of the supported clusters on monolayer MoS_2. Therefore, we performed *ab initio* MD simulations using the Nosé algorithm[53] with a cutoff energy of 200 eV to explore possible structures of the Au_3 and Au_4 clusters deposition on monolayer MoS_2. The simulation length was 10 ps with a time step of 1 fs at the temperature of 600 K. Then, some possible deposition configurations were sampled from the results of the MD simulations every 50 steps, result in 200 initial configurations for each MD process. Further structural optimizations using more accurate settings (see above) were performed to determine the typical stable configurations. Similar approaches have been employed to investigate other complicated systems, including CrW_2O_9/MgO(001),[54,55] Au/TiO_2 and Au/ZrO_2(101).[38]

The role of the van der Waals correction was investigated using three vdW correction methods as follows: DFT-D2 [56] and DFT-D3 [57] with pairwise force field method proposed by Grimme and co-workers. The optB86b-vdW method proposed by Lundqvist and co-workers, in which the vdW contribution is expressed directly as a function of the electron density.[58] In addition to van der Waal correction which is crucial to well describe the interaction between the cluster and substrate at the interface, the electronic structures for the adsorbed Au_n clusters may be affected by the onsite correction to the strong correlated d electrons. Actually, test calculations using GGA + U method combined with projected augmented wave (PAW) were also performed, and our results indicated that GGA and GGA + U methods yielded similar results of configurations and electronic structure including total of Bader charge, the atomic Bader charge of adsorbed Au_n cluster, total magnetization, the total DOSs and particle DOSs projected on the S 3p, Mo 4d, Au 6s and 5d orbitals in the present work.

3 Results and discussion

3.1 Structures of Au_n ($n = 1–4$) clusters in the gas phase

Before considering the cases of supported gold clusters, we first discuss the structures of Au_n ($n = 1–4$) clusters in gas phase. Many experimental[59–64] and theoretical works[51,52,65–67] have been devoted to the structures and stability of gold clusters. Schaaff *et al.*[60] have isolated five massive gold-cluster molecules in high yield and the electronic structure of these molecules has been deduced by optical absorption spectroscopy. Zanti *et al.*[51] have obtained the structures of small gold clusters Au_n ($n \leq 16$) using density functional theory at B3LYP level. Lee *et al.*[52] further explore the relative stabilities and electronic properties of small

neutral and anionic gold clusters (Au_n and Au_n^-, $n = 4–7$) using high-level CCSD(T) calculations with large basis sets. In here, the geometry and the stability of Au_n ($n = 1–4$) clusters (placed in a $20 \times 20 \times 20$ Å cubic box) are reexamined at the PBE level with a plane-wave basis set. The calculated structures of ground state and low-lying isomers with corresponding structural parameters and relative energies are shown in Fig. 1. For Au_2 cluster (Fig. 1b), the calculated Au–Au bond length is 2.53 Å, which is in agreement with the reported experimental value (2.47 Å).[68] For Au_3 cluster, there are two low-lying isomers. Fig. 1c shows that the ground state of Au_3 cluster is V-shaped structure (C_{2v} symmetry) with two Au–Au bonds (2.56 Å) and the bond angle of 137.7°. Other Au_3 isomer (Fig. 1d) is triangular geometry with D_{3h} symmetry, which is 0.11 eV higher in energy than that of the V-shaped Au_3 cluster. Each Au–Au bond length of the equilateral triangle Au_3 cluster is 2.67 Å. The order of the stability for the Au_3 cluster is consistent with that obtained by Zanti *et al.* using B3LYP method with an atomic orbital basis set.[51] In the case of Au_4 cluster, there are four low-lying isomers: rhombic Au_4, Y-shaped Au_4, zigzag Au_4 and tetrahedral Au_4. The ground state of Au_4 cluster (Fig. 1e) is rhombic with C_s symmetry. The bond lengths of Au–Au bonds at four side of rhombic Au_4 cluster are all 2.69 Å and the length of diagonal Au–Au bond is 2.63 Å. The second low-lying isomer (Fig. 1f) is Y-shaped structure (C_{2v} symmetry), which is just 0.04 eV higher in energy than that of the rhombic Au_4 cluster. The calculated order of the stability for rhombic Au_4 and Y-shaped Au_4 is in agreement with the result at CCSD(T) level reported by Lee *et al.*[52] While the third low-lying Au_4 isomer (Fig. 1g) is Zigzag structure with C_s symmetry, whose energy is 0.41 eV higher than that of the ground state of Au_4 cluster. It can be seen that rhombic Au_4 cluster, Y-shaped Au_4 cluster and Zigzag Au_4 cluster are separated just by small energy differences. Thus, it can be expected that the interconversion of one isomer into another may occur among the three low-lying isomers of Au_4 cluster. The fourth Au_4 isomer with highly symmetric T_d tetrahedral structure (Fig. 1h) has also been considered. It is the first occurring of 3D geometry of gold clusters. However, it is unstable in consequence of Jahn–Teller distortions, significantly 1.27 eV in energy higher with respect to the ground state of Au_4 cluster.

3.2 Structures of Au_n ($n = 1–4$) clusters supported on monolayer MoS_2

3.2.1 DFT-PBE adsorption results without vdW interactions. The deposition configurations of Au_n ($n = 1–4$) clusters on monolayer MoS_2 at the PBE level are shown in Fig. 2. For the deposition of Au atom on monolayer MoS_2 (Fig. 2a), we found that Au atom preferentially interacts with monolayer MoS_2 at the S-top site with the bond length of 2.37 Å, and the corresponding adsorption energy is 0.63 eV. For Au_2 cluster supported on monolayer MoS_2 (Fig. 2b), it can be seen that Au_2 cluster also prefers to bind vertically on the S-top sites of the monolayer MoS_2 *via* one Au atom. The bond distance of S–Au bond is 2.30 Å, which is shorter than that in Au_1/MoS_2 system (2.37 Å), suggesting the stronger interaction between the Au_2 cluster and monolayer MoS_2. Not surprisingly, corresponding adsorption energy of the supported Au_2 cluster on monolayer MoS_2 (1.02 eV) is 0.39 eV higher in energy than that of supported Au atom. While for Au_3 cluster supported on monolayer MoS_2, we notice that Au_3 cluster assumes two different structures (Fig. 2c and d). In the first configuration M1 (Fig. 2c), after adsorption on monolayer MoS_2, the Au_3 cluster completely loses the initial V-shaped structure in gas phase and forms a triangular structure taking a vertical orientation. The triangular Au_3 cluster is bound to the surface with two Au atoms coordinated to two S atoms, respectively, with average bond lengths of 2.36 Å. And the corresponding adsorption energy is 1.37 eV. In contrast, in model M2 (Fig. 2d), the supported Au_3 cluster maintains the V-shaped structure in gas phase. In this structure, two terminal Au atoms in V-shaped Au_3 cluster bind to two surface S atoms with vertical deposition mode. The average bond length of the two Au–S bonds (2.38 Å) is 0.02 Å longer than that of model M1, indicating weaker Au–S bonds compared with that of model M1. The adsorption energy is 1.31 eV. At the PBE level, the energy difference between the model M1 and M2 is no more than 0.06 eV. While for the case of Au_4/MoS_2 systems, the deposition structures are more complicated, the ground state and low-lying structures within 0.50 eV are presented in Fig. 2e–g. In model M1 (Fig. 2e), the Au_4 cluster loses initial rhombic structure in gas phase and forms a Y-shaped geometry. The Y-shaped Au_4 cluster is vertically supported on monolayer MoS_2 by forming two Au–S bonds with the bond lengths of
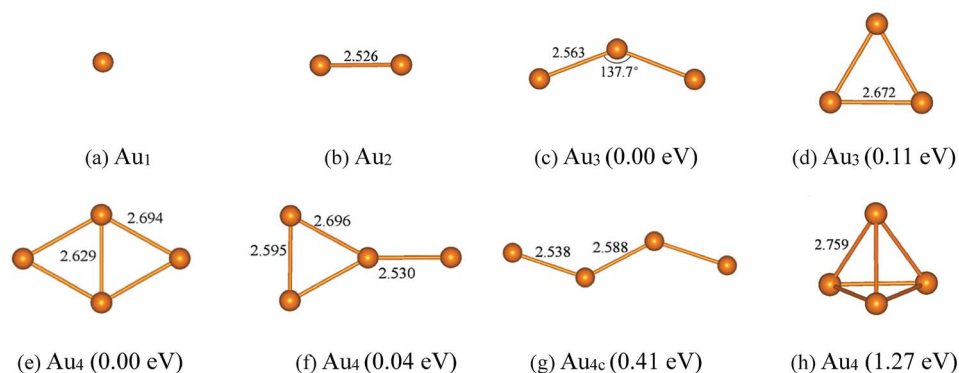

Fig. 1 The optimized structures and their relative energies of Au_n ($n = 1–4$) clusters. Selected bond lengths are given in angstroms and bond angles in degrees.
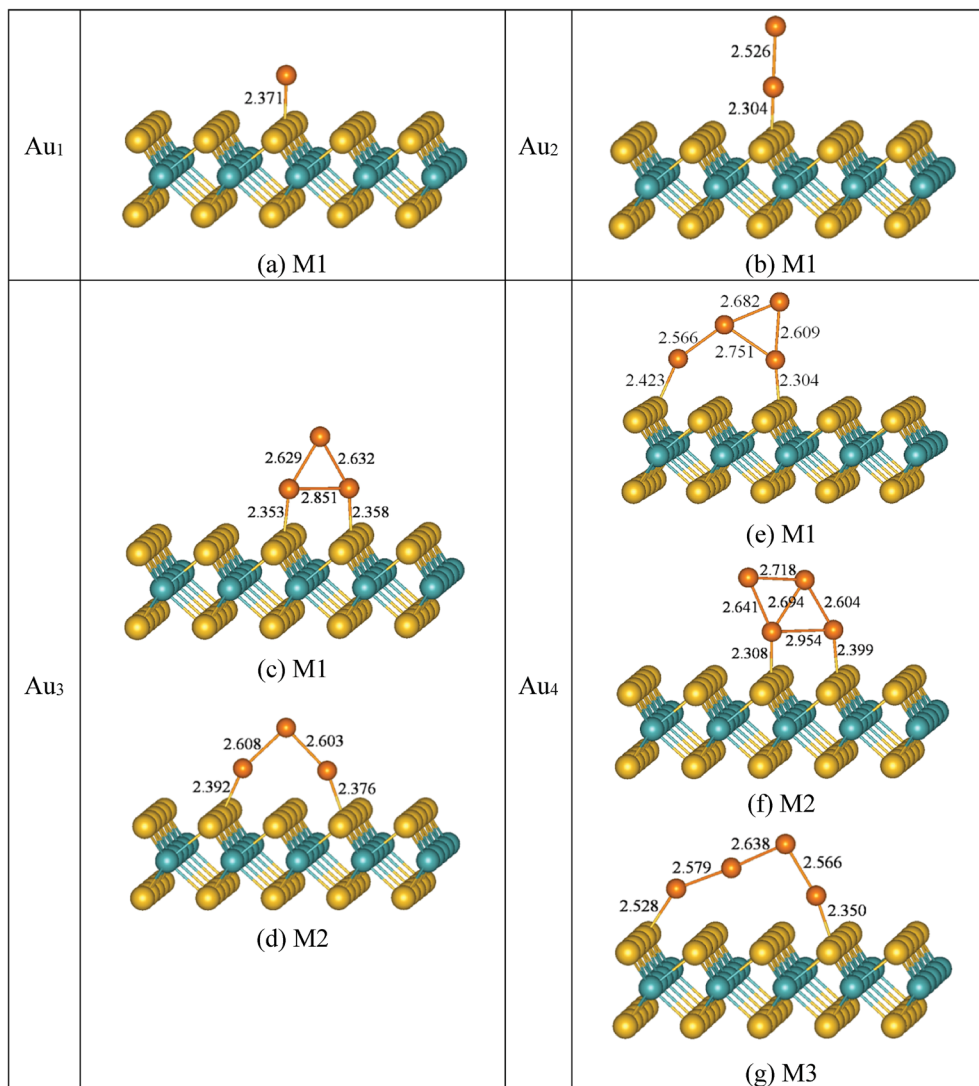
Fig. 2 Optimized structures of Au_n ($n = 1-4$) clusters adsorption on monolayer MoS_2. Color coding: orange, Au atoms; yellow, S atoms; cyan, Mo atoms. Selected bond lengths are given in angstroms.

2.42 Å and 2.30 Å, respectively. In the model M2 (Fig. 2f), after the Au_4 cluster deposition on monolayer MoS_2, the rhombic structure of Au_4 cluster in gas phase is maintained. Two neighbouring Au atoms are bonded to two surface S atoms with bond lengths of 2.31 Å and 2.40 Å, respectively. While for model M3, unlike the M1 and the M2, after deposited on the monolayer MoS_2, the Au_4 cluster is distorted and elongated, resulting in linear configuration. The linear Au_4 cluster is also vertically adsorbed on monolayer MoS_2 by two terminal Au atoms bound with two surface S atoms with the bond lengths of 2.53 Å and 2.35 Å, respectively. Moreover, a three-dimensional supported structure with a tetrahedral shape is also investigated. We found that it is unstable on monolayer MoS_2. This is true at all levels of theory considered (with and without vdW forces). This phenomenon has been reported for Au_4 cluster on TiO_2 and $ZrO_2(101)$ surface.[38] Now let us discuss the relative stabilities of above three deposition configurations for Au_4/MoS_2 systems. The adsorption energies of the three structures are listed in

Table 1. The model M1 is preferred ($E_{ads} = 1.48$ eV) compared to M2 and M3. The model M2 with the adsorption energy of 1.39 eV is only 0.09 eV higher in energy than that of model M1. While for model M3 ($E_{ads} = 0.99$ eV), it is the most unstable structure, which is 0.49 eV and 0.40 eV higher in energy than that in model M1 and M2, respectively. It is clear that the M1 which is originated from the unstable Au_4 isomer in gas phase (Fig. 1f) shows the best thermodynamical stability, while the M2 model which is derived with the most stable cluster in gas phase (Fig. 1e) now is higher in energy (0.09 eV) than M1. Therefore, the relative stability of Au_4 isomer in gas phase is exchanged after depositing on the monolayer MoS_2, indicating a possible way to stabilize the unstable clusters in the gas phase by choosing a suitable support from a thermodynamical point of view.

3.2.2 Adsorption results with vdW interaction. Next, we will discuss the effects of van der Waals forces for the adsorption of Au_n ($n = 1-4$) clusters on monolayer MoS_2 using several vdW

Table 1 Adsorption energy (E_{ads}) and the average bond length of Au–S bond ($\bar{d}$(Au–S)) for Au$_n$ ($n = 1$–4) clusters deposited on monolayer MoS$_2$ with and without the inclusion of van der Waals forces

		$E_{ads}{}^a$ (eV)				$\bar{d}$ (Au–S) (Å)			
		PBE	PBE-D2	PBE-D3	optB86b-vdW	PBE	PBE-D2	PBE-D3	optB86b-vdW
Au$_1$/MoS$_2$	M1	0.63	1.23	1.07	0.97	2.37	2.31	2.33	2.35
Au$_2$/MoS$_2$	M1	1.02	1.76	1.56	1.41	2.30	2.25	2.27	2.29
Au$_3$/MoS$_2$	M1	1.37	2.69	2.36	2.14	2.36	2.29	2.32	2.34
	M2	1.31	2.80	2.39	2.13	2.38	2.33	2.35	2.37
Au$_4$/MoS$_2$	M1	1.48	3.09	2.67	2.29	2.36	2.30	2.33	2.35
	M2	1.39	2.91	2.51	2.17	2.35	2.27	2.31	2.33
	M3	0.99	2.82	2.33	1.90	2.44	2.37	2.40	2.42

^{a} The E_{ads} in this table is defined as $E_{ads} = E_{MoS_2(001)} + E_{Au_n(n = 1-4) \text{ clusters}} - E_{Au_n/MoS_2}$, where E_{MoS_2}, $E_{Au_n(n = 1-4) \text{ clusters}}$, E_{Au_n/MoS_2} and n represent the total energies of the monolayer MoS$_2$, the ground states of Au$_n$ ($n = 1$–4) clusters in the gas phase, the entire systems after depositing Au$_n$ ($n = 1$–4) clusters on monolayer MoS$_2$ and the number of metal atoms in the cluster, respectively.

inclusive DFT schemes (PBE-D2, PBE-D3 and optB86b-vdW). It can be seen that the structures change only slightly after inclusion of vdW forces, with the largest difference being of 0.08 Å. As displayed in Table 1 and Fig. 3, we found that the van der Waals correction increased the adsorption energies for all Au$_n$ ($n = 1$–4)/MoS$_2$ systems with the relative order of adsorption energies of E_{ads}(PBE-D2) > E_{ads}(PBE-D3) > E_{ads}(optB86b-vdW) > E_{ads}(PBE). It can be seen clearly that there is a trend that the PBE-D2 method provides the largest correction to the strength of dispersion interactions, whereas optB86b-vdW gives the smallest. For Au atom deposition on the monolayer MoS$_2$, the adsorption energy goes from 0.63 eV (PBE) to 1.23 eV (PBE-D2), 1.07 eV (PBE-D3), and 0.97 eV (optB86b-vdW), with the relative order of E_{ads}(PBE-D2) > E_{ads}(PBE-D3) > E_{ads}(optB86b-vdW) > E_{ads}(PBE). Like the Au atom, the same trend can also be found for Au$_2$/MoS$_2$ system, the PBE-D2 method gives the largest vdW correction with the adsorption energy of 1.76 eV and optB86b-vdW gives the smallest (1.41 eV), while PBE-D3 method gives the value of adsorption energy (1.56 eV) located just between PBE-D2 method and optB86b-vdW method. Considering supported Au$_3$ cluster, the inclusion of the vdW forces has a stronger effect on the Au$_3$/MoS$_2$ systems with the shorter bond distance of Au–S bond. Therefore, the adsorption energy is

much increased, for model M1 from 1.37 eV (PBE) to 2.69 eV (PBE-D2), 2.36 eV (PBE-D3), and 2.14 eV (optB86b-vdW), and for model M2 from 1.31 eV (PBE) to 2.80 eV (PBE-D2), 2.39 eV (PBE-D3) and 2.13 eV (vdW-DF), with an increase in the adsorption energies of around 56% – 114%. In addition, interestingly, compared with PBE results, the order of stability of model M1 and M2 at the PBE-D2 and PBE-D3 levels is changed. At PBE level the preferred structure is the triangular shape, the model M1, whereas at PBE-D2 and PBE-D3 levels the preferred structure becomes the V-shaped, model M2. However, there is no change in the order of stability of the two low-lying structures for Au$_3$/MoS$_2$ systems at vdW-DF level. This effect is not observed for Au atom and Au$_2$ deposition on the monolayer MoS$_2$. While for Au$_4$/MoS$_2$ systems, when the long-range terms are included, the adsorption energies are increased with the relative order of E_{ads}(PBE-D2) > E_{ads}(PBE-D3) > E_{ads}(optB86b-vdW) > E_{ads}(PBE), in line with the results obtained from other Au$_n$ ($n = 1$–3) clusters on monolayer MoS$_2$. Differently from Au$_3$/MoS$_2$ systems, the order of stability of Au$_4$/MoS$_2$ systems is maintained with the order of M1 > M2 > M3. But the energy difference among the three structures has changed. Once vdW contributions are considered, the energy difference between M1 and M2 becomes larger (0.18 eV, 0.16 eV and 0.12 eV at PBE-D2, PBE-D3 and optB86b-vdW level, respectively, *versus* 0.09 eV at PBE level). Whereas energy difference between M1 and M3 becomes smaller (0.27 eV, 0.34 eV and 0.39 eV at PBE-D2, PBE-D3 and vdW-DF level, respectively, *versus* 0.49 eV at PBE level).

To summarize, for Au$_n$ ($n = 1$–4) clusters on monolayer MoS$_2$, we observed that the geometric structures change only slightly after inclusion of vdW forces, the largest difference being of 0.08 Å. While the van der Waals effects make the major corrections to the adsorption energies, with the relative order of E_{ads}(PBE-D2) > E_{ads}(PBE-D3) > E_{ads}(optB86b-vdW) > E_{ads}(PBE). The PBE-D2 method provides the largest correction to the strength of dispersion interactions, whereas optB86b-vdW gives the smallest. After inclusion of the van der Waals correction, it can also change the order of relative stability and the energy differences of various deposition configurations.
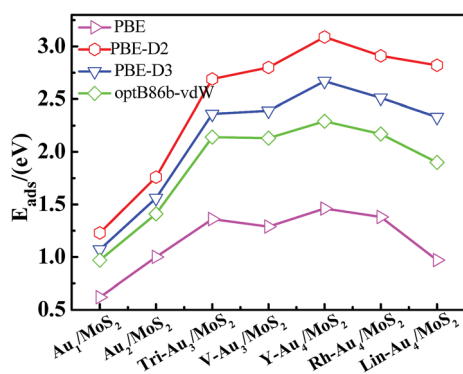

Fig. 3 The adsorption energies of supported Au$_n$ ($n = 1$–4) clusters obtained at PBE, DFT-D2, DFT-D3 and optB86b-vdW (pink, red, dark blue and green polylines, respectively).

3.3 Electronic structures of Au_n ($n = 1–4$) clusters supported on monolayer MoS_2

To better investigate the effects introduced by the deposition of Au_n ($n = 1–4$) clusters on the monolayer MoS_2, in this section, we will focus on the electronic structures of Au_n ($n = 1–4$)/MoS_2 systems. The density of state (DOS) curves displayed in Fig. 4 are the individual spin-up and spin-down densities of states obtained from the spin-polarized calculations at the PBE level, which are almost the same with and without vdW contributions.

3.3.1 Density of states (DOS). Fig. 4a and b displayed the total DOSs and Partial DOSs projected on the S 3p and Mo 4d orbital for the clean monolayer MoS_2, it can be seen that monolayer MoS_2 is a semiconductor in which the valence band (VB) and conduction band (CB) are dominated by S 3p and Mo 4d states, respectively. Fig. 4c presents the total density of state (TDOS) of most stable configuration for Au_1/MoS_2 system. A distinct feature is that a spin-up peak appears near the Fermi level and a spin-down peak occurs at higher energy (about 0.37 eV) in the band gap, which is significantly different from the case on the perfect monolayer MoS_2. Clearly, the system of supported Au atom with odd number atom is spin polarized with the total magnetic moment of 1.0 μ_B. According to the partial density of states (PDOSs) of S 3p, Mo 4d, Au 6s and 5d orbital (Fig. 4d), it is clear that the above asymmetrical peaks are mainly derived from Au 6s state. Fig. 4d also shows that the 5d state of Au atom is overlapped with S 3p state at a wide energy range (from −4.5 eV to −1 eV), indicating a strong hybridization between Au and surface S atom. Similar phenomenon is also observed for another gold cluster with odd number of atoms, Au_3/MoS_2 system (see Fig. 4g and h). Whereas, things are radically different in the supported gold cluster with even number of atoms. For the supported Au_2 cluster with even number of Au atoms, the DOS curves as shown in Fig. 4e can be seen that, differently from the supported Au and Au_3 atom, the most stable configuration of Au_2/MoS_2 system is non-spin polarized due to the closed-shell nature of the Au_2 cluster. An obvious characteristic is that a new symmetrical sharp feature is present near the Fermi level. Further partial density of states (PDOSs) of S 3p, Mo 4d, Au 6s and 5d orbital (Fig. 4f) show that the new peak is dominated by Au 6s and 5d states. And the electronic states of Au_2 cluster mixed with the top of the S 3p valence band. Similar phenomenon is also observed for another gold cluster with even number of atoms, Au_4 cluster supported on the monolayer MoS_2 (see Fig. 4i and j).

3.3.2 Bader charges. We further performed Bader charge analysis[69–71] to investigate the bonding nature and charge transfer at interfaces for all the adsorption systems. The results of Bader charge with and without vdW contributions are shown in Fig. 5 and summarized in Table 2. First, we discuss the Bader charges obtained by PBE method. At the PBE level, it is shown that, for the Au_n ($n = 1, 2, 4$)/MoS_2 system, the direction of charge transfer at the interfaces is from the substrate to the supported gold clusters. It is suggested that Au nanoclusters impose remarkable p-doping effects to the monolayer MoS_2, which is in good agreement with that reported in previous experiments.[72] The magnitudes of charge transfer are all small
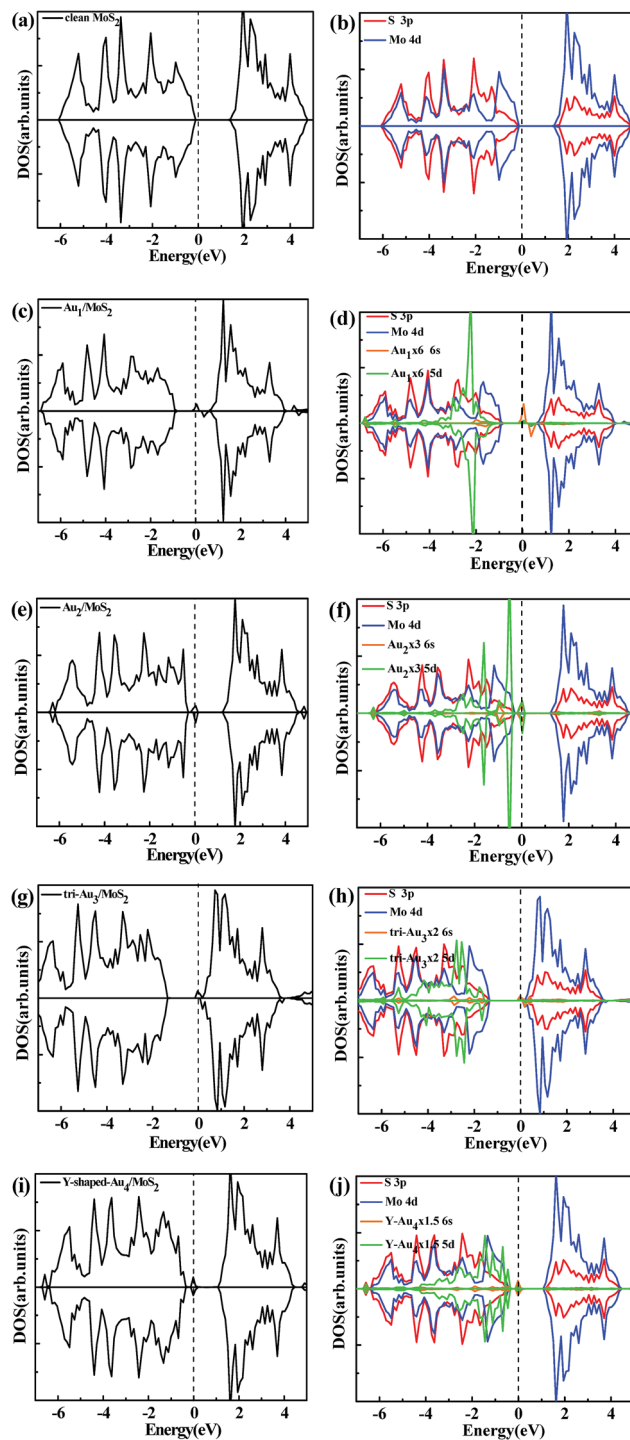

Fig. 4 Total DOSs (a) and partial DOSs projected on the S 3p and Mo 4d of the clean monolayer MoS_2 (b), total DOSs and partial DOSs projected on the S 3p, Mo 4d, Au 6s and 5d of the most stable configurations of Au_1/MoS_2 (c, d), Au_2/MoS_2 (e, f), typical configurations of Au_3/MoS_2 (g, h), and typical configurations of Au_4/MoS_2 (i, j). The vertical dashed line indicates the position of the Fermi level, taken as zero energy.

(<0.2e), which are 0.09e, 0.11e and 0.10/0.10/0.10e for supported Au_1, Au_2 and Au_4 clusters, respectively. While for Au_3 clusters supported on monolayer MoS_2 the magnitudes of charge
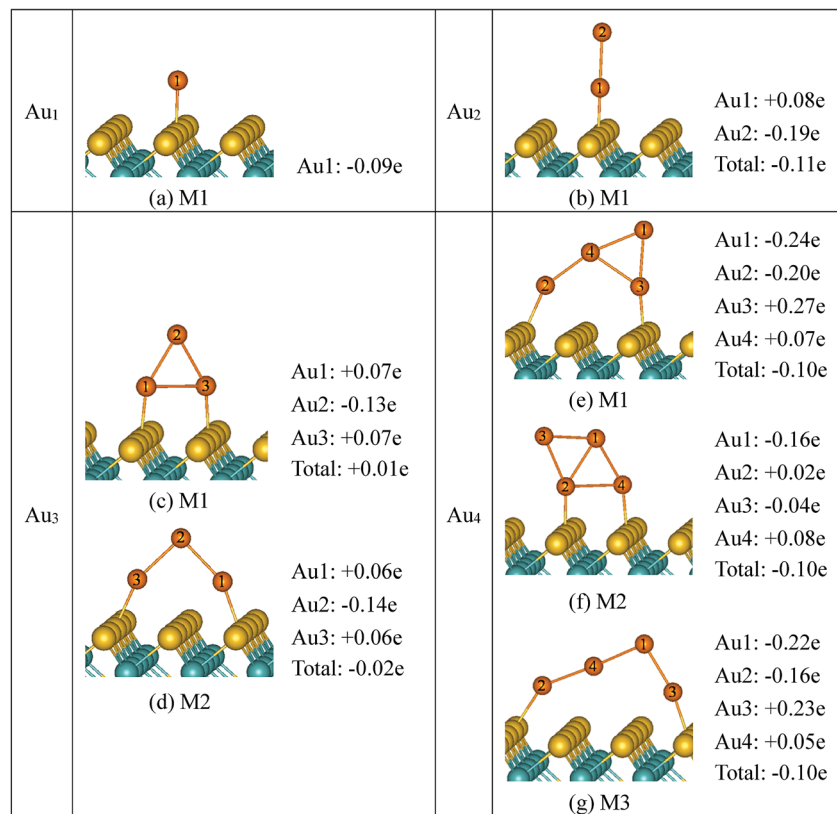
Fig. 5 The Bader charges carried by Au atoms of the supported Au_n ($n = 1–4$) clusters, at PBE level.

transfer are virtually zero. Furthermore, the charge distributions within the Au_n ($n = 2–4$) clusters are also investigated (Fig. 5). It can be seen that, although Au_n ($n = 1–4$) clusters obtained electrons or virtually zero after deposition on the monolayer MoS_2, the magnitudes of charge transfer are mainly obtained by the top Au atom which is far away from the monolayer MoS_2. Whereas most of Au atoms bonded with the surface (at the interface) become positive, which is consistent with the experimental result that hot electron is transferred from Au rods to MoS_2 nanosheets.[37] As shown in Fig. 5b, for Au_2/MoS_2 system, the magnitude of charge on Au(1) atom which is

bound to monolayer MoS_2 is small and positive: $q = +0.08e$, whereas the top Au atom (Au(2) atom) is negatively charged with $q = −0.19e$. For Au_3/MoS_2 (Fig. 5c and d), although the charge transfers between the Au_3 clusters and monolayer MoS_2 are virtually zero, the top Au atom (Au(2) atom) holds negative charge with $q = −0.13/−0.14e$, whereas the Au atoms (Au(1) atom and Au(3) atom) binding to the monolayer MoS_2 are positive, with $q = +0.07e/0.06e$. In terms of the Au_4 clusters, the analysis of charge distributions within the Au_4 cluster shows that, still, there is an accumulation of charge on the top Au atoms ($−0.24e$, $−0.16e$, $−0.22e$ at M1, M2 and M3, respectively).

Table 2 The net Bader charges (ΔQ) of Au_n ($n = 1–4$) clusters deposited on monolayer MoS_2 with and without the inclusion of van der Waals forces

		ΔQ^a (e)			
	Structures	PBE	PBE-D2	PBE-D3	optB86b-vdW
Au_1/MoS_2	M1	−0.09	−0.11	−0.02	−0.05
Au_2/MoS_2	M1	−0.11	−0.15	−0.06	−0.09
Au_3/MoS_2	M1	0.01	0.02	0.02	0.00
	M2	−0.02	−0.04	−0.03	−0.02
Au_4/MoS_2	M1	−0.10	−0.12	−0.12	−0.13
	M2	−0.10	−0.13	−0.15	−0.07
	M3	−0.10	−0.07	−0.08	−0.09

^{a} The negative values indicate that the electrons are transferred from the monolayer MoS_2 to the Au_n ($n = 1–4$) clusters.

Table 3 Adsorption energy (E_{ads}) and the bond length of Au–O bond and O–O bond for O_2 adsorption on Au_n ($n = 1–4$)/MoS_2

	E_{ads}^a (eV)	d (Au–O) (Å)	d (O–O) (Å)
Free O_2	—	—	1.23
Clean MoS_2	0.02	—	1.24
Au_1/MoS_2	1.04	2.07	1.30
Au_2/MoS_2	0.23	2.20	1.26
Au_3/MoS_2	0.64	2.25, 2.26	1.32
Au_4/MoS_2	0.26	2.21	1.26

^{a} The E_{ads} in this table is defined as $E_{ads} = E_{Au_n/MoS_2} + E_{O_2} − E_{O_2/Au_n/MoS_2}$, where E_{Au_n/MoS_2}, E_{O_2}, $E_{O_2/Au_n/MoS_2}$ and n represent the total energies of the most stable Au_n ($n = 1–4$)/MoS_2 system, the ground state of O_2, the entire system after depositing O_2 on Au_n ($n = 1–4$)/MoS_2, and the number of metal atoms in the cluster, respectively.

The results of Bader charge with the inclusion of van der Waals are also shown in Table 2. Clearly, the inclusion of van der Waals forces has no significantly effects on the Bader charges, with the Bader charge difference always smaller than $0.07e$.

3.4 Adsorption and activation of O_2 on Au_n ($n = 1–4$)/MoS_2

To study the effect of the monolayer MoS_2 support on the catalytic properties of the small gold clusters, we performed investigation of adsorption and activation of O_2 on the most stable adsorption configurations of Au_n ($n = 1–4$)/MoS_2 systems. Fig. 6 presents the optimized geometries of O_2 adsorption on Au_n ($n = 1–4$)/MoS_2 systems. It can be seen clearly that, for all Au_n ($n = 1–4$)/MoS_2 systems, O_2 molecule prefers to adsorb on the top Au atom of the supported gold cluster which holds main negative charge. For O_2 adsorption on Au_1/MoS_2 system, O_2 is adsorbed on the Au_1/MoS_2 system by forming one O–Au bond (2.07 Å) with the angle of 116.6° between the O–O and Au–O bonds. The O–O bond is elongated to 1.30 Å (1.23 Å in gas O_2 molecule), indicating activation of O_2 molecule. The adsorption energy is 1.04 eV. Similar results are also observed when O_2 adsorbed on the supported Au_3 cluster with odd number of Au atoms. Two O atoms are bonded with the top Au atom of supported Au_3 cluster which holds more negative charge, forming two Au–O bonds (2.25 Å, 2.26 Å, respectively), with the corresponding adsorption energy of 0.64 eV. After adsorption, O–O bond is elongated to 1.32 Å, indicating significantly activation

of adsorbed O_2 molecule. Whereas, the situation is significantly different for O_2 adsorption on supported Au_2 and Au_4 clusters with even number of Au atoms. After adsorption, O_2 molecule via one O atom interacts with the top Au atom of the supported Au_2 and Au_4 clusters, with the bond length of Au–O bond of 2.20 Å and 2.21 Å respectively. The corresponding O–O bonds are almost not changed with the bond length of 1.26 Å compared with that in free gas O_2. Corresponding adsorption energy is small (0.23 eV and 0.26 eV) for Au_2 clusters and Au_4 clusters, respectively. Since there is another Au atom at the interface (Au_2 atom) in Au_4/MoS_2 system holds some negative charge ($-0.20e$), we also investigated the adsorption configuration when O_2 interacts with Au_2 atom which holds some negative charge. However, strong repulsive forces between surface S atoms and O_2 molecule make the adsorption configuration not stable (not shown).

In short, the above calculations for O_2 adsorption show that the adsorption energies for O_2 adsorption on the Au_1/MoS_2 and Au_3/MoS_2 systems with odd number of Au atoms are much higher than that on the Au_2/MoS_2 and Au_4/MoS_2 systems with even number of Au atoms (1.04 eV, 0.64 eV for Au and Au_3, respectively. 0.23 eV, 0.26 eV for Au_2 and Au_4, respectively), indicating stronger adsorption properties and activation for oxygen molecule on Au_n ($n = 1, 3$)/MoS_2 system with odd number of gold atoms. It is provide a key insight in elucidating the catalytic activity of supported gold clusters with an odd-even
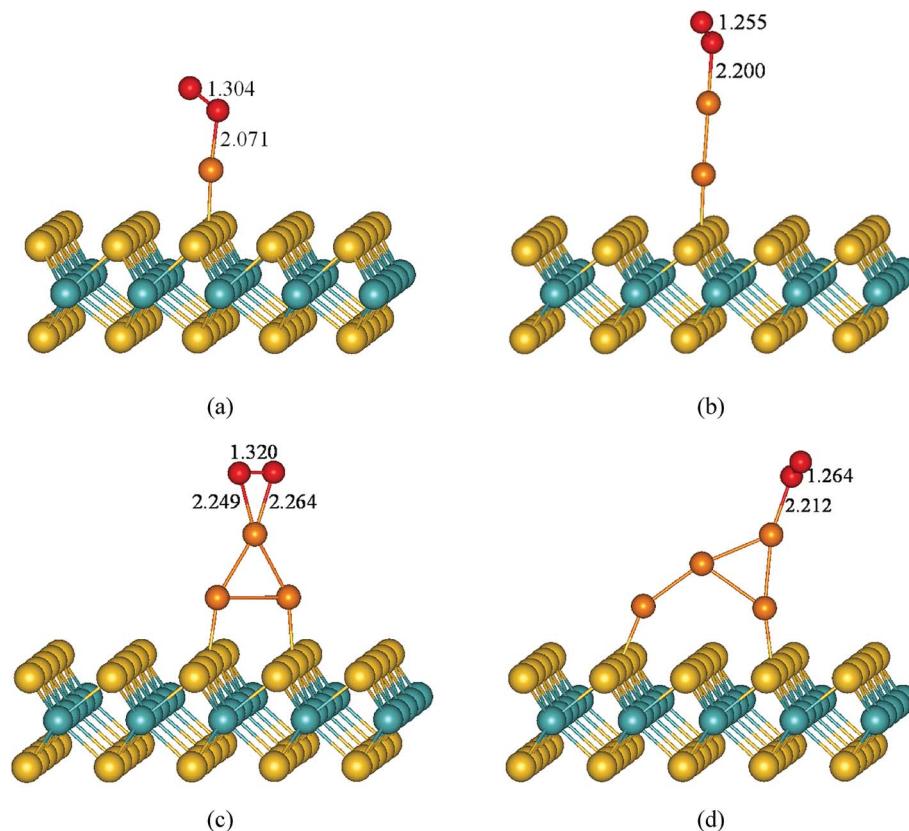

Fig. 6 Optimized structures of O_2 adsorbed on the most stable supported Au_n ($n = 1–4$) clusters. Color coding: orange, Au atoms; yellow, S atoms; cyan, Mo atoms; red, O atoms. Selected bond lengths are given in angstroms.

alternation as a function of the number of gold atoms. This phenomenon has been reported for O_2 molecule adsorption on the free gold clusters.[73–75]

To gain more insight into the origin of the activity of Au_n ($n = 1$–4)/MoS_2, we observed the electronic structures of O_2 adsorption on Au_n ($n = 1$–4)/MoS_2 systems. It is well-known that the singly occupied molecular orbital (SOMO) and the unoccupied one of the O_2 triplet ground state are both antibonding $2\pi^*$ orbital. The spin-up $2\pi^*$ orbital of free O_2 is occupied and located below the Fermi level, while the spin-down $2\pi^*$ orbital of that is unoccupied and located above the Fermi level. We present the partial density of states (PDOS) projected on O_2 molecule and supported Au_n ($n = 1$–4) clusters in Fig. 7. Clearly, when O_2 interacts with supported Au_n ($n = 1$–4) clusters, the 5d and 6s state of Au atom is mixed with 1π and $2\pi^*$ orbitals of the adsorbed O_2, indicating bonding of Au and O_2. Now the spin-down $2\pi^*$ orbital of adsorbed O_2 appears partial population, indicated charge transfer occurring from the supported Au atom to the antibonding $2\pi^*$ orbital of the adsorbed O_2, result in stretching of the O–O bond and the catalytic activation of O_2 molecule (Fig. 6). Furthermore, the charge distribution of adsorbed O_2, its neighbor Au atoms and Au_n ($n = 1$–4) clusters were calculated using Bader charge analysis, as listed in Table 4. The charge values of the supported Au_n ($n = 1$–4) clusters before O_2 adsorption are in the range of $-0.09e$ to $-0.11e$ except virtually zero for Au_3 cluster. After adsorption of O_2 molecule, more electrons are transferred from supported gold clusters to O_2 molecule, result in supported gold clusters become positive charge in the range of $+0.11e$ to $+0.35e$. Further atomic Bader charge analysis (Table 4) shows that the values of charge

Table 4 Bader charges of gold clusters (Au_n), neighboring gold atom (Au) and oxygen molecule

	Substrate without O_2		Substrate with O_2		
	$\Delta Q(Au_n)$	$\Delta Q^a(Au)$	$\Delta Q(Au_n)$	$\Delta Q^b(Au)$	$\Delta Q(O_2)$
Au_1/MoS_2	−0.09	−0.09	+0.35	+0.35	−0.39
Au_2/MoS_2	−0.11	−0.19	+0.11	+0.23	−0.14
Au_3/MoS_2	+0.01	−0.13	+0.25	+0.30	−0.38
Au_4/MoS_2	−0.10	−0.24	+0.16	+0.20	−0.18

[a] $\Delta Q(Au)$ and. [b] $\Delta Q(Au)$ represent the charge value of the top Au atom which prefer to interact with O_2, respectively.

obtained by O_2 molecule mainly come from its neighboring Au atom which bonded to O_2 molecule. It also can be seen clearly from the electron charge density difference of O_2/Au_n (1–4)/MoS_2 (Fig. 8). The isosurface of an excess of the electron density is mainly localized on O_2, while the plot of the electron density loss is on the Au atom directly interacting with O_2 molecule. This is consistent with above analysis of charge transfer from the supported neighboring gold clusters to O_2 molecule. Therefore, it is very clear that adsorption and activation of O_2 molecule are strongly influenced by the top Au atom which holds more negative charge. In addition, the values of charge obtained by O_2 molecule from supported Au_1 ($-0.39e$) and Au_3 clusters ($-0.38e$) are larger than that from supported Au_2 cluster ($-0.14e$) and Au_4 cluster ($-0.18e$), which are responsible for better catalytic activation of the adsorbed oxygen molecule. Note that from electron charge density difference (Fig. 8) there is more electron density localized on the O_2/Au_n ($n = 1, 3$)/MoS_2
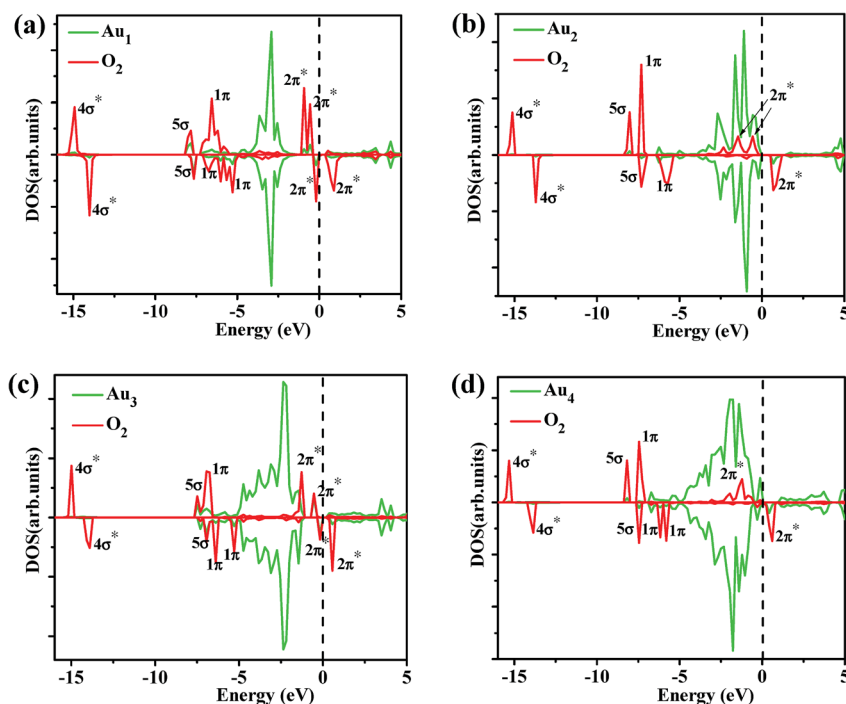

Fig. 7 Partial DOSs projected on the O_2 molecule and Au_n ($n = 1$–4) clusters of O_2 adsorption on Au_1/MoS_2 (a), Au_2/MoS_2 (b), Au_3/MoS_2 (c), and Au_4/MoS_2 (d). The vertical dashed line indicates the position of the Fermi level, taken as zero energy.
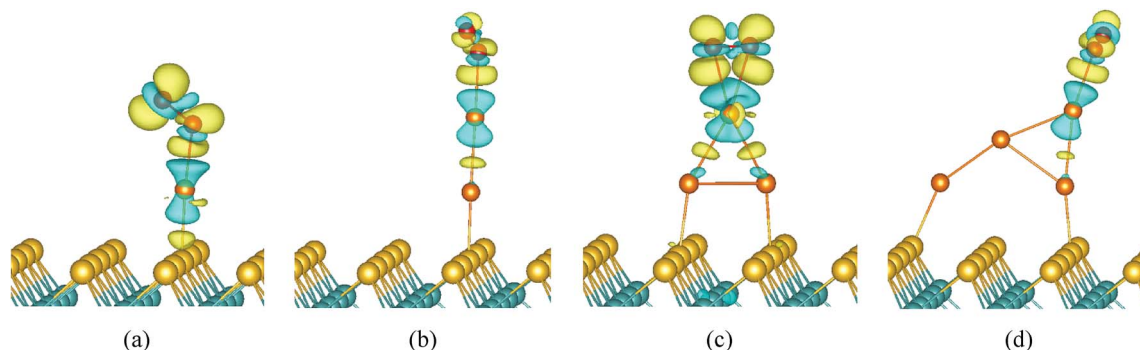
Fig. 8 Isosurfaces plot of the electron charge density difference for O_2 molecule on (a) Au_1/MoS_2, (b) Au_2/MoS_2, (c) Au_3/MoS_2, (d) Au_4/MoS_2, i.e., $\rho_{tot}(O_2/Au_n/MoS_2) - \rho_{tot}(O_2) - \rho_{tot}(Au_n/MoS_2)$. The contours shown are at ±0.003 e $Å^{-3}$, respectively. Blue regions correspond to electron loss, and yellow ones correspond to electron accumulation.

systems with odd number of Au atoms than that on the O_2/Au_n ($n = 2, 4$)/MoS_2 systems with even number of Au atoms. This phenomenon corresponds to the above analysis of charge transfer from the supported gold clusters to O_2 molecule.

4   Conclusions

In the present work, we studied the structures, electronic properties and catalytic properties of Au_n ($n = 1–4$) clusters supported on monolayer MoS_2 using DFT calculations with and without the inclusion of van der Waals (vdW) forces, including PBE, PBE-D2, PBE-D3 and optB86b-vdW methods. We found that all Au_n ($n = 1–4$) clusters are preferentially vertically adsorbed on monolayer MoS_2 by Au–S bonds. The relative stability of Au_n ($n = 1–4$) clusters in gas phase is not preserved after landing on the monolayer MoS_2, indicating a possible way to stabilize the unstable clusters in the gas phase by choosing a suitable support from a thermodynamical point of view. The van der Waals correction increased the adsorption energies for all supported Au_n ($n = 1–4$) clusters with the relative order of adsorption energies of E_{ads}(PBE-D2) > E_{ads}(PBE-D3) > E_{ads}(optB86b-vdW) > E_{ads}(PBE). The van der Waals effects make the major corrections to the adsorption energies, and can also change the order of stability and the energy differences of various deposition configurations. The Bader charge analysis shows that, although the directions of charge transfer is from supported monolayer MoS_2 to supported Au_n ($n = 1–4$) clusters for all adsorption configurations, the top Au atoms far from the monolayer MoS_2 hold main negative charge whereas most of Au atoms at the interface become positive charged. It is demonstrated that the excess of the negative charges obtained by the top Au atom can considerably promote the adsorption and catalytic activation of O_2 on the supported Au_n ($n = 1–4$) clusters, due to the charge transfer occurring from the top Au atom to the O_2 $2\pi^*$ antibonding orbital, result in the elongation of the O–O bond and activation of O_2. Furthermore, our results represent better adsorption properties and catalytic activities of adsorbed O_2 on supported Au_1 and Au_3 clusters with magnetic properties, with respect to that on supported Au_2 and Au_4 clusters with nonmagnetic properties. The current study provides further insight into the adsorption and catalysis

properties of small Au_n ($n = 1–4$) clusters supported on monolayer MoS_2, in which play a crucial role in the activation of O_2. More works are necessary to study the structure and the electronic properties to clearly see whether the number-dependent adsorption properties still holds when larger Au_n nanocluster ($n > 4$) supported on monolayer MoS_2

Conflicts of interest

There are no conflicts to declare.

Acknowledgements

References

1   C. R. Henry, *Surf. Sci. Rep.*, 1998, **31**, 231–233.

2   G. Ertl and H. J. Freund, *Phys. Today*, 1999, **52**, 32–38.

3   B. Yoon, H. Hakkinen, U. Landman, A. S. Worz, J. M. Antonietti, S. Abbet, K. Judai and U. Heiz, *Science*, 2005, **307**, 403–407.

4   C. Zhang, B. Yoon and U. Landman, *J. Am. Chem. Soc.*, 2007, **129**, 2228–2229.

5   H. Y. Kim, H. M. Lee and G. Henkelman, *J. Am. Chem. Soc.*, 2012, **134**, 1560–1570.

6   Z. P. Liu, S. J. Jenkins and D. A. King, *Phys. Rev. Lett.*, 2005, **94**, 196102.

7   Q. Fu, H. Saltsburg and M. Flytzani-Stephanopoulos, *Science*, 2003, **301**, 935–938.

8   T. Mark, B. G. Vladimir, P. H. V. Owain, A. Pavel, B. G. Angel, S. T. Mintcho, F. G. J. Brian and M. L. Richard, *Nature*, 2008, **454**, 981–983.

9 H. Falsig, B. Hvolbaek, I. S. Kristensen, T. Jiang, T. Bligaard, C. H. Christensen and J. K. Nørskov, *Angew. Chem., Int. Ed.*, 2008, **120**, 4913–4917.

10 H. Häkkinen, S. Abbet, A. Sanchez, U. Heiz and U. Landman, *Angew. Chem., Int. Ed.*, 2003, **42**, 1297–1300.

11 A. Roldán, S. González, J. M. Ricart and F. Illas, *ChemPhysChem*, 2009, **10**, 348–351.

12 B. Yoon, P. Koskinen, B. Huber, O. Kostko, B. von Issendorff, H. Hakkinen, M. Moseler and U. Landman, *ChemPhysChem*, 2007, **8**, 157–161.

13 N. Lopez and J. K. Nørskov, *J. Am. Chem. Soc.*, 2002, **124**, 11262–11263.

14 I. N. Remediakis, N. Lopez and J. K. Nørskov, *Angew. Chem., Int. Ed.*, 2005, **117**, 1858–1860.

15 B. Yoon, H. Häkkinen, U. Landman, A. S. Wörz, J.-M. Antonietti, S. Abbet, K. Judai and U. Heiz, *Science*, 2005, **307**, 403–407.

16 Z. P. Liu, X. Q. Gong, J. Kohanoff, C. Sanchez and P. Hu, *Phys. Rev. Lett.*, 2003, **91**, 266102.

17 L. M. Molina and B. Hammer, *J. Chem. Phys.*, 2005, **123**, 161104.

18 A. Roldán, J. M. Ricart, F. Illas and G. Pacchioni, *J. Phys. Chem. C*, 2010, **114**, 16973–16978.

19 D. Matthey, J. G. Wang, S. Wendt, J. Matthiesen, R. Schaub, E. Lægsgaard, B. Hammer and F. Besenbacher, *Science*, 2007, **315**, 1692–1696.

20 S. Laursen and S. Linic, *Phys. Rev. Lett.*, 2006, **97**, 026101.

21 B. T. Teng, J.-J. Lang, X. D. Wen, C. Zhang, M. Fan and H. G. Harris, *J. Phys. Chem. C*, 2013, **117**, 18986–18993.

22 G. J. Hutchings, M. S. Hall, A. F. Carley, P. Landon, B. E. Solsona, C. J. Kiely, A. Herzing, M. Makkee, J. A. Moulijn, A. Overweg, J. C. Fierro-Gonzalez, J. Guzman and B. C. Gates, *J. Catal.*, 2006, **242**, 71–81.

23 L. Fu, N. Q. Wu, J. H. Yang, F. Qu, D. L. Johnson, M. C. Kung, H. H. Kung and V. P. Dravid, *J. Phys. Chem. B*, 2005, **109**, 3704–3706.

24 S. Stankovich, D. A. Dikin, G. H. B. Dommett, K. M. Kohlhaas, E. J. Zimney, E. A. Stach, R. D. Piner, S. T. Nguyen and R. S. Ruoff, *Nature*, 2006, **442**, 282–286.

25 E. Gracia-Espino, G. Hu, A. Shchukarev and T. Wagberg, *J. Am. Chem. Soc.*, 2014, **136**, 6626–6633.

26 P. Vogt, P. D. Padova, C. Quaresima, J. Avila, E. Frantzeskakis, M. C. Asensio, A. Resta, B. Ealet and G. L. Lay, *Phys. Rev. Lett.*, 2012, **108**, 155501.

27 G. Kim, A. R. Jang, H. Y. Jeong, Z. Lee, D. J. Kang and H. S. Shin, *Nano Lett.*, 2013, **13**, 1834–1839.

28 M. Gao, A. Lyalin and T. Taketsugu, *J. Phys. Chem. C*, 2012, **116**, 9054–9062.

29 T. Liao, Z. Sun and S. X. Dou, *ACS Appl. Mater. Interfaces*, 2017, **9**, 8255–8262.

30 L. Sheng, T. Liao, L. Kou and Z. Sun, *Mater. Today Energ.*, 2017, **3**, 32–39.

31 T. Liao, Z. Sun, C. Sun, S. X. Dou and D. J. Searles, *Sci. Rep.*, 2014, **4**, 6256.

32 A. K. Geim and K. S. Novoselov, *Nat. Mater.*, 2007, **6**, 183–191.

33 A. K. Geim, *Science*, 2009, **324**, 1530–1534.

34 K. F. Mak, C. Lee, J. Hone, J. Shan and T. F. Heinz, *Phys. Rev. Lett.*, 2010, **105**, 136805.

35 M. Chhowalla, H. S. Shin, G. Eda, L. J. Li, K. P. Loh and H. Zhang, *Nat. Chem.*, 2013, **5**, 263–275.

36 J. Zhu, H. Zhang, Y. Tong, L. Zhao, Y. Zhang, Y. Qiu and X. Lin, *Appl. Surf. Sci.*, 2017, **419**, 522–530.

37 Y. Shi, J. Wang, C. Wang, T.-T. Zhai, W. J. Bao, J. J. Xu, X. H. Xia and H. Y. Chen, *J. Am. Chem. Soc.*, 2015, **137**, 7365–7370.

38 A. R. Puigdollers, P. Schlexer and G. Pacchioni, *J. Phys. Chem. C*, 2015, **119**, 15381–15389.

39 J. Carrasco, W. Liu, A. Michaelides and A. Tkatchenko, *J. Chem. Phys.*, 2014, **140**, 084704.

40 G. Kresse and J. Hafner, *Phys. Rev. B: Condens. Matter Mater. Phys.*, 1994, **49**, 14251–14269.

41 G. Kresse and J. Furthmüller, *Comput. Mater. Sci.*, 1996, **6**, 15–50.

42 G. Kresse and J. Furthmüller, *Phys. Rev. B: Condens. Matter Mater. Phys.*, 1996, **54**, 11169–11186.

43 P. E. Blöchl, *Phys. Rev. B: Condens. Matter Mater. Phys.*, 1994, **50**, 17953–17979.

44 G. Kresse and D. Joubert, *Phys. Rev. B: Condens. Matter Mater. Phys.*, 1999, **59**, 1758–1775.

45 J. P. Perdew, K. Burke and M. Ernherhof, *Phys. Rev. Lett.*, 1996, **77**, 3865–3868.

46 P. Joensen, E. D. Crozier, N. Alberding and R. F. Frindt, *J. Phys. C: Solid State Phys.*, 1987, **20**, 4043–4053.

47 D. Le, T. B. Rawal and T. S. Rahman, *J. Phys. Chem. C*, 2014, **118**, 5346–5351.

48 Q. Chen, Y. Ouyang, S. Yuan, R. Li and J. Wang, *ACS Appl. Mater. Interfaces*, 2014, **6**, 16835–16840.

49 D. Ma, Y. Tang and G. Yang, *Appl. Surf. Sci.*, 2015, **328**, 71–77.

50 C. Ataca and S. Ciraci, *J. Phys. Chem. C*, 2011, **115**, 13303–13311.

51 G. Zanti and D. Peeters, *Theor. Chem. Acc.*, 2013, **132**, 1300.

52 H. M. Lee and K. S. Kim, *Chem.–Eur. J.*, 2012, **18**, 13203–13207.

53 S. Nosé, *J. Chem. Phys.*, 1984, **81**, 511–519.

54 J. Zhu, H. Zhang, Y. W. Tong, Y. W. Tong, C. X. Wang, B. Wang, X. Huang and Y. F. Zhang, *J. Chem. Phys.*, 2016, **144**, 174706.

55 J. Zhu, H. Zhang, L. Zhao, W. Xiong, X. Huang, B. Wang and Y. F. Zhang, *Appl. Surf. Sci.*, 2016, **138**, 213–222.

56 S. Grimme, *J. Comput. Chem.*, 2006, **27**, 1787–1799.

57 S. Grimme, J. Antony, S. Ehrlich and H. Krieg, *J. Chem. Phys.*, 2010, **132**, 154104.

58 M. Dion, H. Rydberg, E. Schröder, D. C. Langreth and B. I. Lundqvist, *Phys. Rev. Lett.*, 2004, **92**, 246401.

59 C. L. Cleveland, U. Landman, T. G. Schaaff, M. N. Shafigullin, P. W. Stephens and R. L. Whetten, *Phys. Rev. Lett.*, 1997, **79**, 1873–1876.

60 T. G. Schaaff, M. N. Shafigullin, J. T. Khoury, I. Vezmar, R. L. Whetten, W. G. Cullen, P. N. First, C. Gutiérrez-Wing, J. Ascensio and M. J. Jose-Yacamán, *J. Phys. Chem. B*, 1997, **101**, 7885–7891.

61 K. J. Taylor, C. L. Pettiette-Hall, O. Cheshnovsky and R. E. Smalley, *J. Chem. Phys.*, 1992, **96**, 3319–3329.

62 K. Koga, H. Takeo, T. Ikeda and K. Ohshima, *Phys. Rev. B: Condens. Matter Mater. Phys.*, 1998, **57**, 4053–4062.

63 V. A. Spasov, Y. Shi and K. M. Ervin, *Chem. Phys.*, 2000, **262**, 75–91.

64 B. Palpant, B. Prével, J. Lérme, E. Cottancin, M. Pellarin, M. Treilleux, A. Perez, J. L. Vialle and M. Broyer, *Phys. Rev. B: Condens. Matter Mater. Phys.*, 1998, **57**, 1963–1970.

65 M. S. Liao, J. D. Watts and M. J. Huang, *J. Phys. Chem. C*, 2014, **118**, 21911–21927.

66 J. Wang, G. Wang and J. Zhao, *Phys. Rev. B: Condens. Matter Mater. Phys.*, 2002, **66**, 035418.

67 X. B. Li, H. Y. Wang, X. D. Yang, Z.-H. Zhu and Y. J. Tang, *J. Chem. Phys.*, 2007, **126**, 084505.

68 J. L. Jules and J. R. Lombardi, *J. Phys. Chem. A*, 2003, **107**, 1268–1273.

69 R. F. W. Bader, *Chem. Rev.*, 1991, **91**, 893–928.

70 G. Henkelman, A. Arnaldsson and H. Jónsson, *Comput. Mater. Sci.*, 2006, **36**, 354–360.

71 W. Tang, E. Sanville and G. Henkelman, *J. Phys.: Condens. Matter*, 2009, **21**, 084204.

72 Y. Shi, J. K. Huang, L. Jin, Y. T. Hsu, S. F. Yu, L. J. Li and H. Y. Yang, *Sci. Rep.*, 2013, **3**, 1839.

73 A. Lyalin and T. Taketsugu, *J. Phys. Chem. C*, 2009, **113**, 12930–12934.

74 B. Yoon, H. Häkkinen and U. Landman, *J. Phys. Chem. A*, 2003, **107**, 4066–4071.

75 X. L. Ding, Z. Y. Li, J. L. Yang, J. G. Hou and Q. S. Zhu, *J. Chem. Phys.*, 2004, **120**, 9594–9600.